Journal Pre-proof

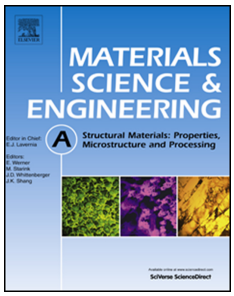

Effects of cold rolling and low-temperature annealing on microstructure and mechanical properties of rapidly solidified Cu–3Ag-0.5Zr alloy

Xiang Wu, Richu Wang, Chaoqun Peng, Yan Feng, Zhiyong Cai

PII: S0921-5093(19)31614-4

DOI: https://doi.org/10.1016/j.msea.2019.138829

Reference: MSA 138829

To appear in: *Materials Science & Engineering A*

Received Date: 1 September 2019

Revised Date: 13 December 2019

Accepted Date: 14 December 2019

Please cite this article as: X. Wu, R. Wang, C. Peng, Y. Feng, Z. Cai, Effects of cold rolling and low-temperature annealing on microstructure and mechanical properties of rapidly solidified Cu–3Ag-0.5Zr alloy, *Materials Science & Engineering A* (2020), doi: https://doi.org/10.1016/j.msea.2019.138829.

Xiang Wu: Material preparing; microstructural characterisation and mechanical testing and other experimental work; data analysis and preparing all tables and figures for the manuscript, writing the manuscript. Richu Wang: Material preparing; experiment design; funding acquisition; project administration. Chaoque Peng: Correction of the original manuscript; Yan Feng: Discussing the research outcomes with the first author. Zhiyong Cai: Supervision; proposal of the research idea; correction of the original manuscript.

Effects of cold rolling and low-temperature annealing on microstructure and mechanical properties of rapidly solidified Cu-3Ag-0.5Zr alloy

Xiang Wu, Richu Wang, Chaoqun Peng, Yan Feng, Zhiyong Cai*

School of Materials Science and Engineering, Central South University, Changsha 410083, China

*Corresponding author. E-mail: zycaimse@163.com (Z.Y. Cai)

Abstract: The effects of cold rolling and low-temperature annealing on the microstructure and mechanical properties of Cu-3Ag-0.5Zr alloy prepared by gas atomization and hot isostatic pressing (HIP) were investigated. The HIPed alloy provides a fine and homogeneous microstructure for the subsequent rolling. The high density of dislocations, the large number of ultrafine grains, and the interaction between dislocations and fine precipitates (nano-sized Ag and micro-sized Cu_4AgZr) are responsible for the high hardness (193 Hv), excellent tensile strength (654 MPa), but relatively low elongation (5.6%). Low-temperature annealing achieves a desirable combination of high strength and moderate elongation. After annealing at 350 °C for 2 h, the tensile strength, yield strength and elongation are 584 MPa, 534 MPa and 13%, respectively. When annealed for 8 h, the tensile strength and yield strength decrease to 558 MPa and 504 MPa, respectively, while the elongation recovers to 16.5%. The increased elongation is mainly attributed to the recovery of dislocation-accumulation ability and the slight grain growth.

Key words: Cu-3Ag-0.5Zr alloy; Rapid solidification; Cold rolling; Annealing; Microstructure; Mechanical properties

1. Introduction

Cu-Ag-Zr alloys are used extensively in the fields of electric railway, pulsed high field magnets and cooled combustion chamber applications owing to the good combination of strength, ductility and conductivity [1-4]. Among them, the Cu-3Ag-0.5Zr alloy (in weight percentage) is well developed for fabricating rocket engine combustion chambers which serve at high temperature and pressure. The high strength of this alloy is mainly attributed to the strengthening effect of Ag precipitates and Cu-Ag-Zr intermetallic compounds, while the high conductivity is ascribed to the low solubility of Ag and Zr in the Cu matrix at room temperature [5, 6].

Plastic processing is a common method to improve the microstructural homogeneity and mechanical properties of the Cu-3Ag-0.5Zr alloy prepared by conventional casting. Krishna et al. [7] reported that an increment of 160% in yield strength was achieved by rolling at 500 °C compared with the solution-treated Cu-3Ag-0.5Zr alloy, and a good ductility of 23% was retained. Krishna et al. [8] also studied the effects of cold rolling and aging on the tensile properties of the Cu-3Ag-0.5Zr alloy, and they found that the tensile strength and yield strength increased with the amount of cold reduction and reached the maximum values of 529 and 523 MPa, respectively, at 80% reduction. However, the ductility decreased from 47% of the solution-treated sample to 4.8%. After aging at 400 °C for 1 h, a recovered ductility of 12% was obtained at the expense of the slight decrease in yield strength.

Cold rolling can significantly enhance the strength of most alloys, but a strength ceiling is easily reached because of the composition segregation and coarse grains in the initial materials prepared by conventional casting. Therefore, an attempt was made to prepare the initial

Cu-3Ag-0.5Zr alloy with fine and homogeneous microstructure by gas atomization and HIP, followed by cold rolling and low-temperature annealing. The effects of cold rolling and annealing on the microstructural characteristics and mechanical properties were investigated.

2. Experiments

Atomized Cu-3Ag-0.5Zr pre-alloyed powder (~200 mesh) used in this study was produced by vacuum melting-high pressure gas atomization and then filled into a mild steel capsule, followed by degassing and sealing. The details of powder atomization and degassing process are the same as the preparation of the Cu-3Ag-1Zr alloy shown elsewhere [9]. Hot isostatic pressing (HIP) treatment was used to consolidate the powder at 830 °C under 150 MPa for 2 h. The HIPed alloy, used as the initial material, was further rolled at room temperature, achieving 80% reduction in total thickness with a 10% reduction in each pass. The cold rolling (CR) samples were subsequently annealed under argon atmosphere at 350 °C for 0.5, 1, 2, 4, and 8 h, respectively.

The microstructures were examined using field emission scanning electron microscopy (FESEM, Sirion200) operating at 20 kV equipped with energy dispersive spectroscopy (EDS), transmission electron microscopy (TEM, Tecnai G^2 20) operating at 200 kV equipped with EDS, and electron backscatter diffraction (EBSD) system. The samples for SEM were mechanically ground and polished. Samples for TEM and EBSD were thinned to 50-80 μm, followed by twin-jet electro-polishing in a solution of 67 vol.% methanol + 33 vol.% nitric acid, at -30 °C and 10 V. The average grain size was measured by EBSD method and linear intercept method based on ten TEM images of each sample, respectively. The phase identification and crystallographic structure were investigated by X-ray diffraction (XRD, D/max 2550) using Cu Kα radiation (λ=0.1541 nm) with a step size of 4°/min. The microhardness was measured on the well-polished

samples using a Vickers hardness tester (BUEHLER5104) under a load of 100 g for 15 s. The average hardness value was obtained from more than 8 indentations for each sample. The tensile testing at room temperature was performed in a test machine (MTS LANDMARK) at a strain rate of 2 mm/min. Dog-bone shaped samples for tensile tests were cut along the rolling direction with a gauge length of 25 mm and a cross section of 8 mm×2 mm.

3. Results and discussion

3.1 Microstructures before and after cold rolling

Fig. 1(a) shows the EBSD orientation map of the initial material. The map illustrates that the HIPed alloy with nearly equiaxed grains has no crystal preferential orientation. The average grain size is approximately 5.6 μm. Fig. 1(b) shows the back-scattered electron image of the initial material. A large number of white particles with irregular shape ranging from 1 to 5 μm are observed in the matrix (as indicated by the arrows). The corresponding EDS spectrum (Fig. 1(e)) indicates that these irregularly shaped particles are coarse Ag-rich precipitates, which is the result of the segregation of supersaturated solid solution during the HIP process. Generally, these large sized Ag-rich particles have an unsatisfied strengthening effect on Cu-based alloys [10-12]. Besides, finer particles are also found in the back-scattered electron image. These finer particles can be clearly observed by secondary electron images in SEM at high magnification, as shown in Fig 1(c). It is apparent that the white particles approximately 1-3 μm are coarse Ag-rich particles, which are identical to the same particles with irregular shape in Fig. 1(b). In addition, many gray particles having the size smaller than 1 μm can also be observed in the secondary electron image, as indicated by the black arrows. The corresponding EDS qualitative analysis in Fig. 1(f) demonstrates that the gray particles are Cu-Ag-Zr intermetallic. For the small size of the

Cu-Ag-Zr intermetallic particles, it is difficult to get exact atomic ratio by the SEM-EDS results. However, these intermetallic phases named Cu_4AgZr have been reported in our previous research, which is one of the important strengthening phases in the Cu-Ag-Zr alloy [13]. Furthermore, high-density precipitates with a size approximately ~20 nm are distributed uniformly in the matrix (Fig. 1(d)), and the TEM and STEM-HAADF images of these precipitates are displayed in Fig. 2. The selected area diffraction pattern inserted in Fig 2(a) indicates that these nano-sized particles have a cube-on-cube relationship with the Cu matrix, demonstrating that they are continuous Ag precipitates [2, 4, 9].

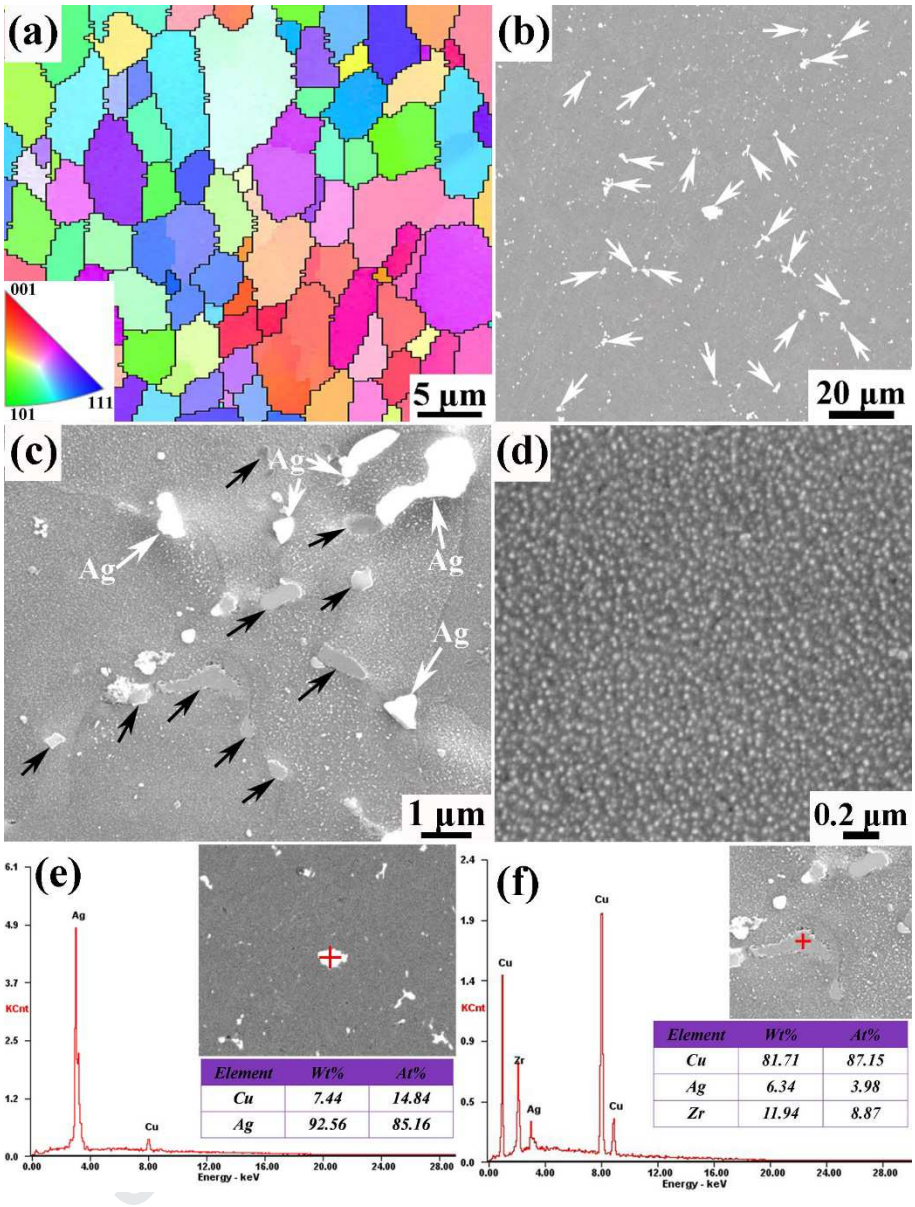

Fig. 1. (a) EBSD orientation map, (b) back-scattered electron image, (c, d) secondary electron images, (e) EDS of coarse Ag-rich particle, and (f) EDS of Cu_4AgZr phase of the initial material.

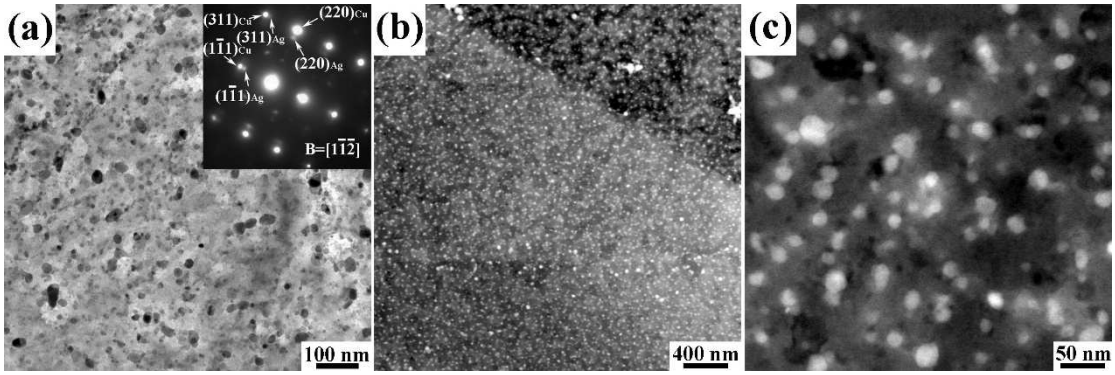

Fig. 2 (a) The TEM image and (b, c) STEM-HAADF images of the continuous Ag precipitates.

Fig. 3 shows the SEM micrographs of the alloy after cold rolling. The coarse Ag-rich particles in the initial material are broken down into nano-sized particles (white) and form banded structures distributing along the rolling direction (RD), and the microstructure is further refined by cold rolling. Furthermore, some gray particles (indicated by black arrows) with the size of 70-200 nm and high density of continuous Ag precipitates are also observed in the matrix (Fig. 3(b)). It is reasonable to presume that the gray particles are Cu_4AgZr phases, and they are formed by the crushed Cu_4AgZr with a relative larger size in the initial alloy, and further verification is needed by TEM observation. While the size and density of the dispersed Ag precipitates do not change appreciably before and after cold rolling.

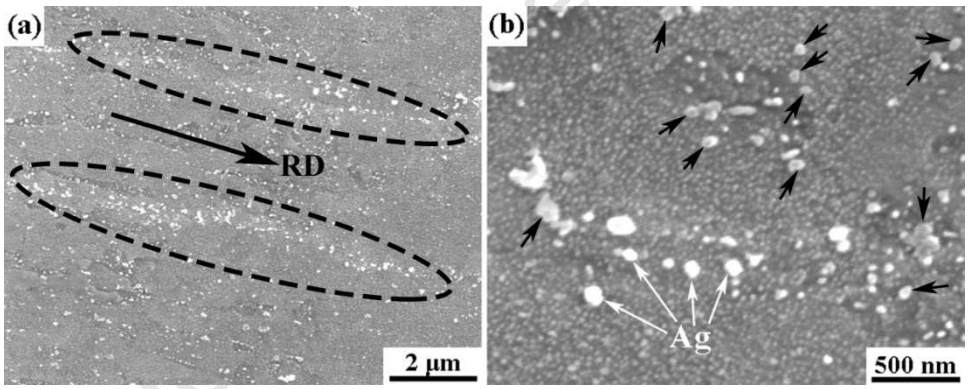

Fig. 3. The secondary electron images of (a) banded structures and (b) nano-sized particles in the CR sample.

Fig. 4 shows the TEM images of the CR sample. The severely deformed microstructure with high density of dislocations and deformation band (DB) is observed (Fig. 4(a)). However, no deformation twins are found, which is mainly attributed to the small initial grain size before cold rolling [14]. Besides, particles approximately 200 nm result in the pile-up of dislocations, as illustrated in Fig. 4(b). The EDS quantitative analysis indicates these micro-sized Cu-Ag-Zr intermetallic compounds contain 74.0 at.% Cu, 9.2 at.% Ag and 16.8 at.% Zr, confirming they are

Cu_4AgZr phases, which is in agreement with several literatures [6, 15]. It implies that the gray particles in Fig. 3(b) are also Cu_4AgZr phases. Furthermore, many dislocation cells occur in the matrix and are trapped by the high density of dispersed particles (Fig. 4(c)). The inserted selected area diffraction pattern (SAPD) in Fig. 4(d) demonstrates that these dispersed particles are continuous Ag precipitates, which can effectively accumulate dislocations [16, 17]. Moreover, the coarse Ag particles in the initial material have been crushed into small particles with a size less than 100 nm. This means that all Ag precipitates are in the nanometer range, which is helpful for achieving a significant strength improvement.

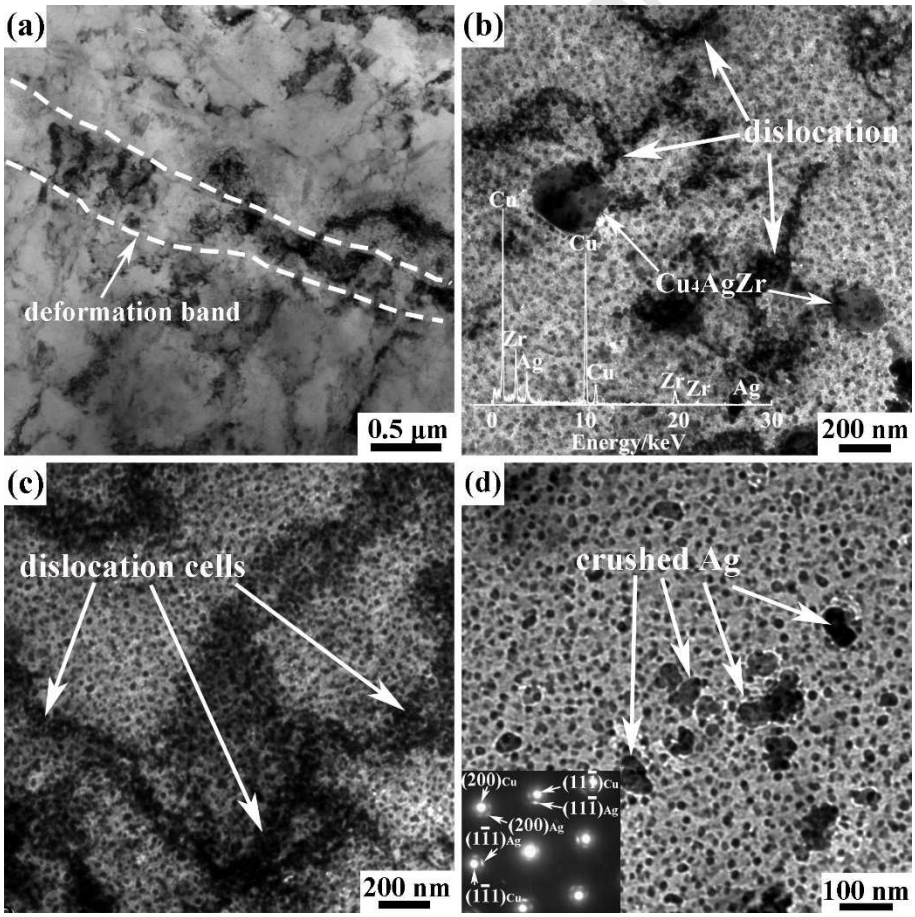

Fig. 4. TEM images of (a) deformation band and ultrafine grains, (b) Cu_4AgZr particles, (c) dislocation cells, and (d) nano-sized Ag precipitates in the CR sample.

3.2 Microstructure evolution during annealing

Fig. 5(a) shows the XRD patterns of the CR sample after annealing at 350 ℃ for various durations. The intensity of the Cu peaks is much higher than that of the Ag peaks due to the low content of Ag in the alloy. In addition, the intensity of the Ag peaks increases gradually as with extending the annealing time due to the precipitation of Ag solutes. Fig. 5(b) shows the slight shift of the Cu (111) peak to high angles during annealing. The similar phenomenon is also observed by other researchers, which is associated with the decreased lattice parameter of the Cu matrix when the Ag solutes gradually precipitate out of the matrix [2, 18].

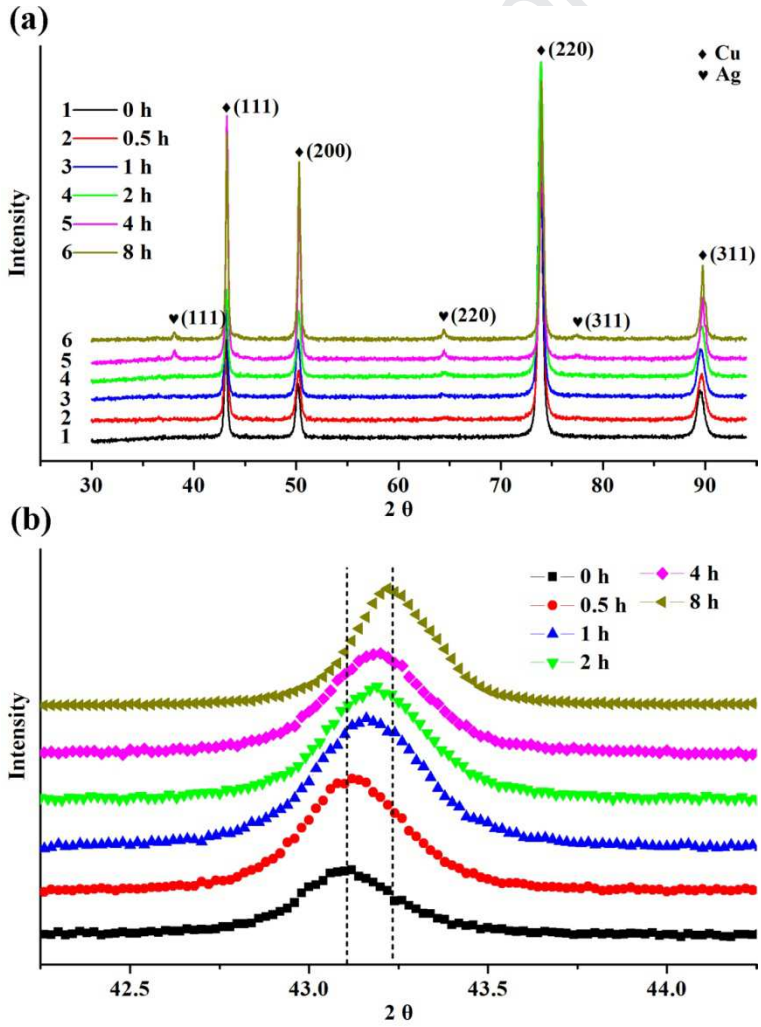

Fig. 5. (a) XRD patterns and (b) Cu (111) peaks of the CR samples annealed at 350 ℃.

The SEM images of the CR sample after annealing at 350 °C for 0.5, 2, 4, and 8 h, respectively, are presented in Fig. 6. When annealed at 350 °C for 0.5 h, the microstructure of the sample under SEM shows insignificant change compared with that of the CR sample. The Cu_4AgZr particles with a size smaller than 200 nm (indicated by the white arrows) and the banded structures consisting of crushed Ag particles are also observed in Fig. 6(a). With increasing the annealing time to 2 h, the banded structures disappear and the microstructure of the alloy is more homogeneous. However, the size of some Cu_4AgZr particles (indicated by white arrows in Fig. 6(b)) increases to 200-600 nm. When the sample is annealed for 4 or 8 h, no further coarsening of the Cu_4AgZr particles is observed, as evident by the white arrows in Fig. 6(c) and (e). In addition, one can separate the SEM microstructure into two main regions when the CR sample is annealed for 4 or 8 h. In Region 1, the continuous Ag precipitates remain fine and stable. While in Region 2, some coarser precipitates can be observed. As depicted in the magnified images of Fig. 6(d) and (f), numerous discontinuous Ag precipitates with lamellar structure are confirmed in Region 2. The lamella thickness of these precipitates is approximately 60 nm, and the length is less than 600 nm. The discontinuous Ag precipitates are commonly observed in the Cu-Ag and Cu-Ag-Zr alloys, and the discontinuously precipitated cells have a lower hardness than the continuously precipitated cells [3, 12, 17, 19-21]. The appearance of the discontinuous Ag precipitates when annealed for more than 4 h may also be related with the accelerated diffusion rate of solution atoms. The heavy cold rolling increases the number of lattice-level defects and improves the distortion energy, leaving the alloy in a state with high free energy, which improves the diffusion rate of solute atoms during annealing.

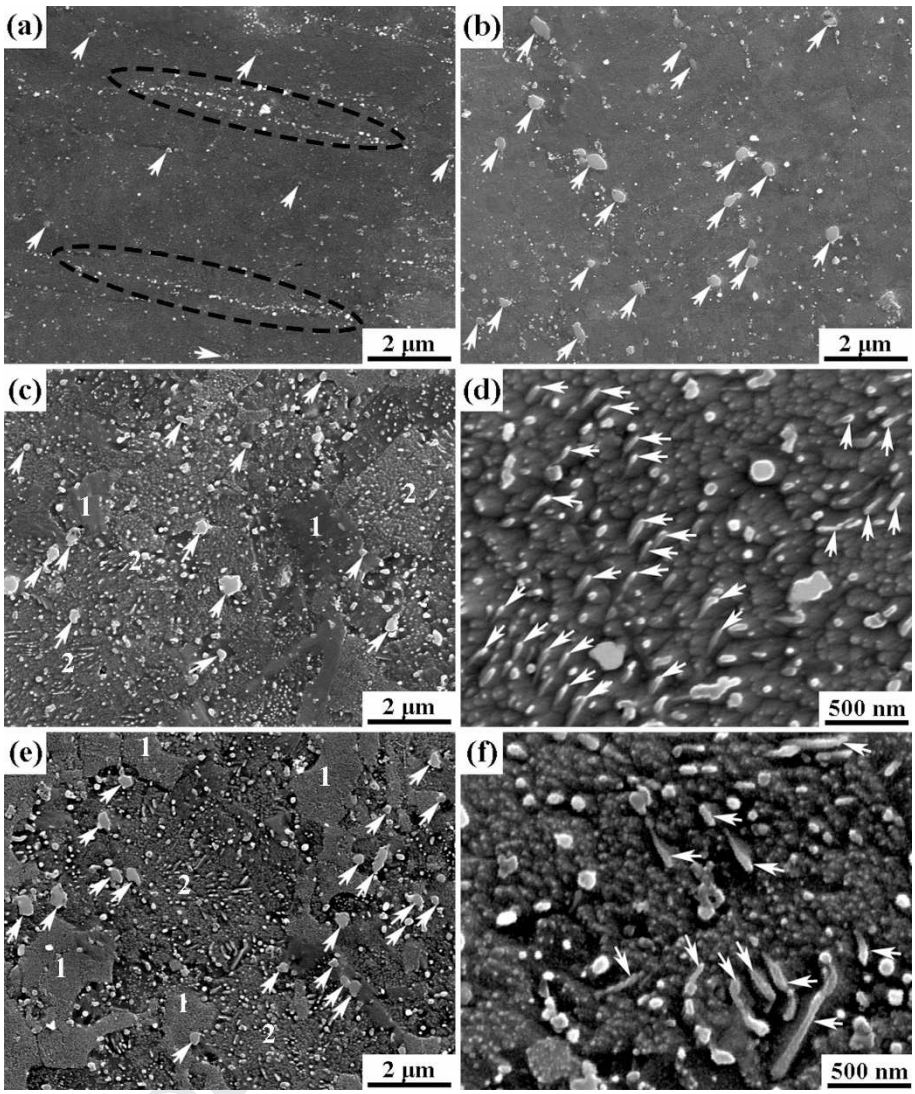

Fig. 6. Secondary electron images of CR samples annealed at 350 °C for (a) 0.5 h, (b) 2 h, (c, d) 4 h, and (e, f) 8 h.

TEM images of the CR sample after annealing at 350 °C for 0.5 and 2 h are presented in Fig. 7. The tangled dislocations and ultrafine sub-grains are observed when the sample is annealed for 0.5 h. However, only a small number of sub-grains have well-defined boundaries. The occurrence of sub-grains is attributed to the rearrangement of dislocations during a short-time annealing [22]. After annealing for 2 h, the dislocation density decreases and a large number of ultrafine grains with well-defined boundaries are observed, as indicated in Fig. 7(d). In addition, annealing twins

with a thickness of 100-150 nm are also observed. It is noted that the nucleation of annealing twins requires the migration of grain boundaries [23-25]. This means that the size of grains was changed during annealing, virtually a slight increment. Furthermore, the size and number density of the continuous Ag precipitates in Fig. 7(c) and (f) do not change appreciably in comparison with those in the CR sample as presented in Fig. 4(d).

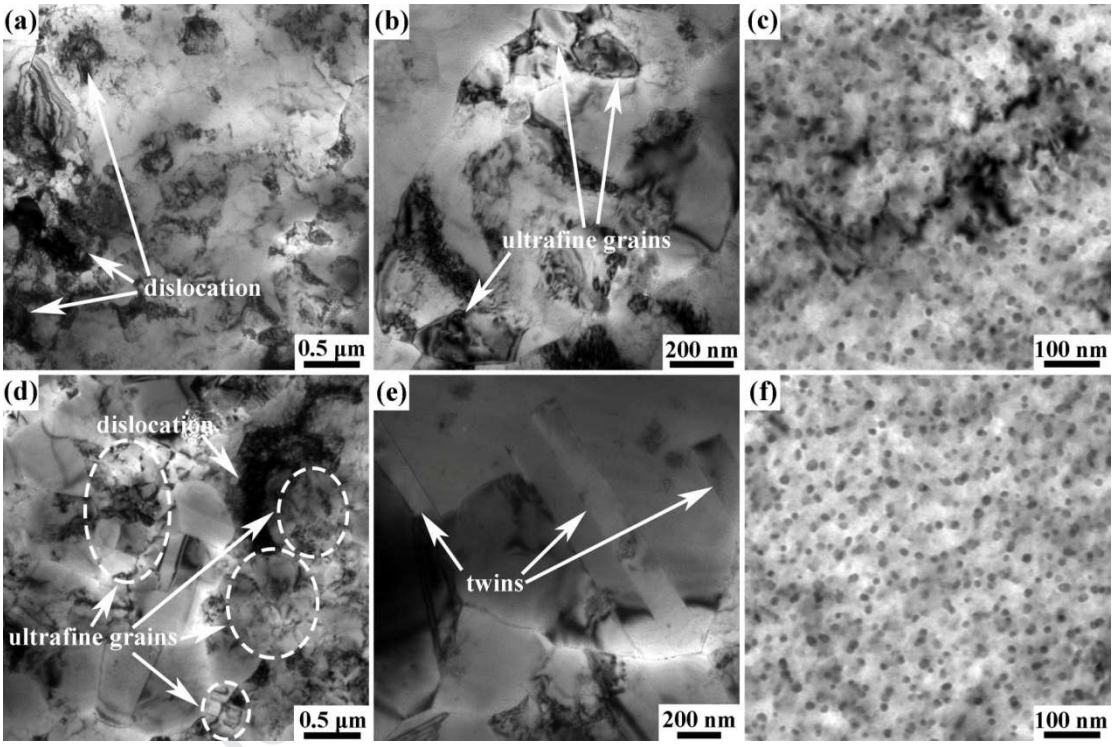

Fig. 7. TEM images of the CR sample annealed at 350 °C for (a-c) 0.5 h, and (d-f) 2 h.

When the sample is annealed for 4 h, significant decreases in the number of ultrafine grains and the density of dislocation are observed in Fig. 8(a). In addition, the formation of discontinuous Ag precipitates with lamellar structure (indicated by dashed oval) and granular shape (indicated by arrows) are confirmed in Fig. 8(b). And these discontinuous Ag precipitates with larger size than that of the continuous Ag precipitates are also observed in Fig. 6(c) and (d). Meanwhile, the size and number density of the continuous Ag precipitates with a dispersed distribution in Fig. 8(c) have an obvious decrease in comparison with those of the sample annealed for 2 h in Fig. 7(f).

This phenomenon may be attributed to the transfer of solute Ag atoms from continuous precipitates with a smaller size to discontinuous precipitates with a coarser size. When further annealed for 8 h, more discontinuous precipitates are present in the matrix, as demonstrated in Fig. 8(d) and (e). While the continuous Ag precipitates even disappear in some grains, and a heterogeneous distribution of the continuous precipitates between different grains is observed in Fig. 8(f).

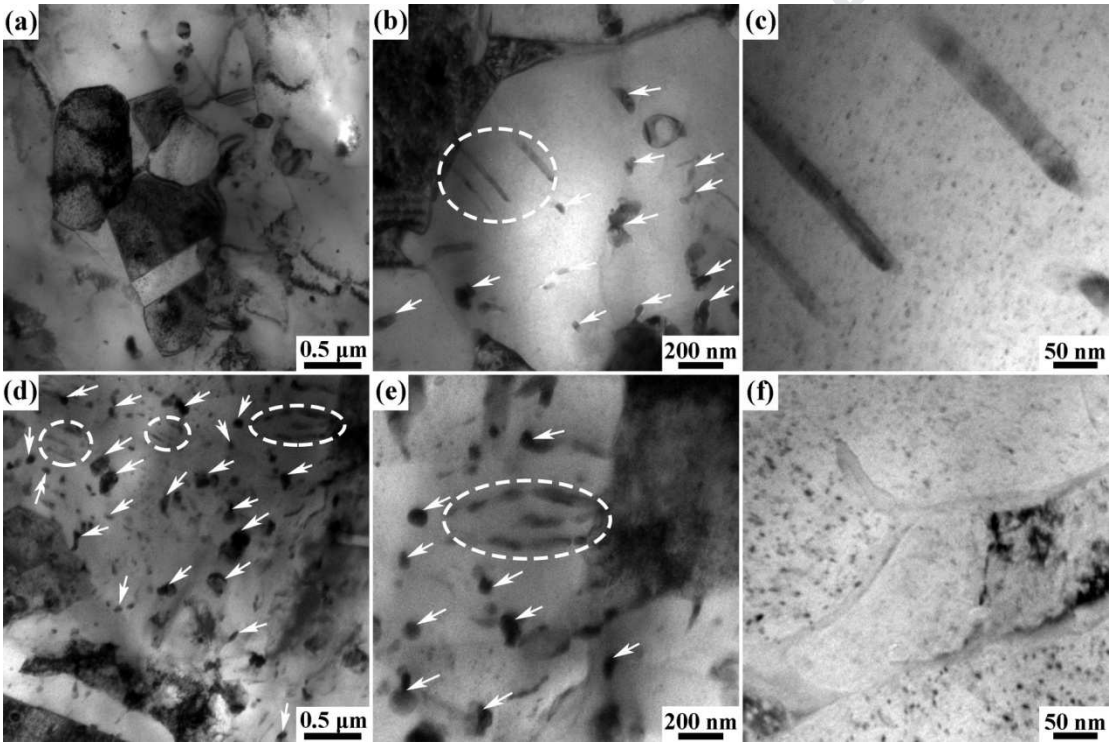

Fig. 8. TEM images of the CR sample annealed at 350 °C for (a-c) 4 h, and (d-f) 8 h.

Figure 9 displays the grain misorientation maps of the CR sample annealed at 350 °C for 2, 4, and 8 h, respectively. The different colors represent different grain orientations depicted in the unit triangle. The microstructure of the annealed samples is dominated by large elongated grains, fine equiaxed grains and deformation band (DB). A large fraction of low angle boundaries (LABs) is existed in the deformation band interior. With the increasing of annealing time, more large-sized grains with high angle boundaries (HABs) are observed.

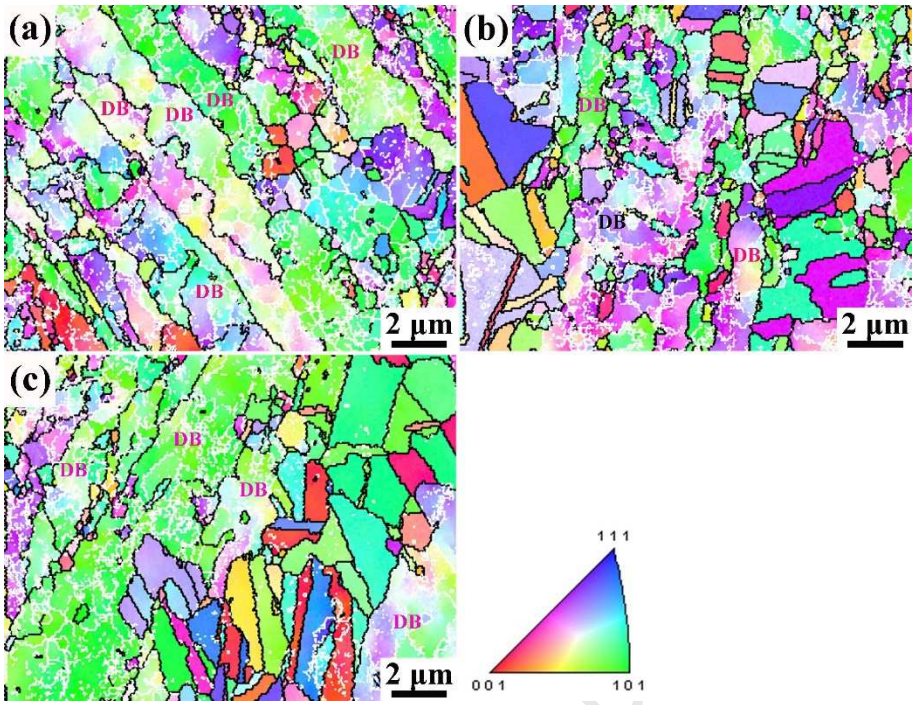

Fig. 9. Inverse pole figures (IPF) of the CR samples annealed at 350 °C for (a) 2 h, (b) 4 h, (c) 8 h. The black lines present HABs (misorientation angle above 15°), and white lines present LABs (misorientation angle between 2° and 15°).

According to the XRD patterns of the annealed samples in Fig. 5, the micro strain (ε) and crystallite size (*d*) are roughly estimated by Williamson-Hall method [26, 27], which is given by:

$$\beta cos\theta = K\lambda/d + (4sin\theta)\cdot\varepsilon \quad (1)$$

Where β is the peak broadening, K is a constant (~0.9), λ is wave length of the Cu Kα radiation (0.1541 nm), and θ is the Bragg angle. The values of the micro strain (ε) and crystallite size (*d*) can be obtained from the slope and intercept of the fitting $\beta\cos\theta - 4\sin\theta$ plot, respectively. Then, the dislocation density (ρ) can be calculated by the following equation [27, 28]:

$$\rho = 2\sqrt{3}\cdot\varepsilon/(db) \quad (2)$$

Where b is the Burgers vector, which calculated by $b = a/\sqrt{2}$ (a is the lattice parameter of

Cu, 0.3615 nm). The estimated dislocation density of the annealed samples is shown in Fig. 10. In addition, the effect of annealing time on the average grain size of the CR sample is also presented in Fig. 10. It is noted that the average grain size of the samples is obtained from the TEM images and EBSD results, respectively. From the comparison of the results obtained by different ways, the EBSD counting provides higher values of grain sizes than the TEM counting. This is because some nano-sized grains are missed to count by EBSD for the step size of 90 nm during scanning, while some large-sized ones are missed to count by TEM observation for the small field of view. It implies that TEM counting method is more suitable for the measurement of nanocrystalline and ultrafine-grained materials. High density of dislocation about 16.7×10^{13} m^{-2} and average grain size approximately 800 nm (measured by TEM counting) are obtained in the CR sample, which is attributed to the fine microstructure of the initial material and the severe deformation. The dislocation density exhibits a significant decreasing trend with increasing the annealing time, while the change of average grain size displays an opposite character. The recovery process during annealing leads to the decrease of dislocation density and the coarsening of grains. Prolonging the annealing time to 8 h, the dislocation density decreases to approximately 9.2×10^{13} m^{-2} and the average grain size increases to approximately 2.7 μm (measured by EBSD).

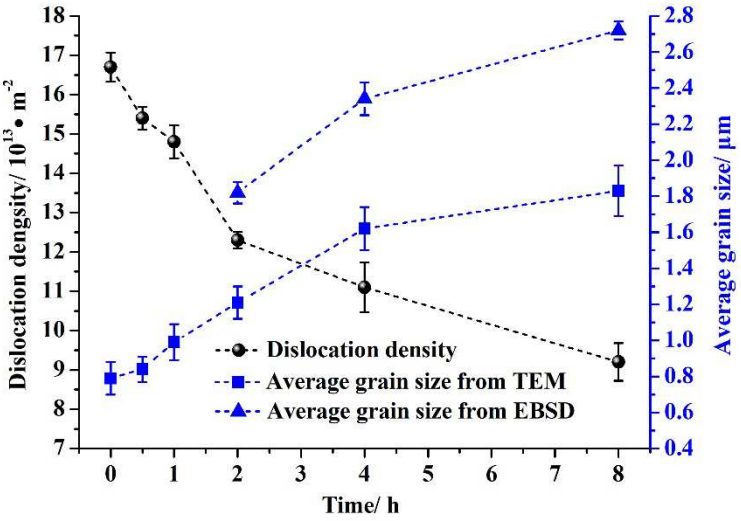

Fig. 10. Effects of annealing time on dislocation density and average grain size of the CR sample.

3.3 Mechanical properties

The mechanical properties of the Cu-3Ag-0.5Zr alloy are evaluated by Vickers microhardness measurements and tensile tests. Figure 11 depicts the variation of hardness as a function of the annealing time (0.5-8 h). The CR sample exhibits a maximum hardness of 193 Hv and then drops with the annealing time. Figure 12(a) displays the typical engineering stress-strain curves of the Cu-3Ag-0.5Zr alloy. The tensile properties obtained from Fig. 12(a) are summarized in Fig. 12(b). One can see that the CR sample exhibits superior ultimate tensile strength (UTS-654 MPa) and yield strength (YS-642 MPa) but lower elongation (EL-5.6%) in comparison with the HIPed alloy (UTS-365 MPa, YS-248 MPa, EL-37.5%), which limits the practical utility because of the unsatisfactory elongation. The strength decreases sharply (UTS-609 MPa, YS-565 MPa) after annealing for 0.5 h due to the recovery of the alloy, and the strength curves show sign of leveling off with increasing the annealing time. However, a significant improvement of ductility is achieved in the samples annealed for 0.5, 1, 2, 4 and 8 h with corresponding elongations of 9%, 11.0%, 13.0%, 15.0% and 16.5%, respectively. The strength and elongation have a relatively low

sensitivity to the further extended annealing time. It is to be noted in this respect that annealing at low temperature for various times can enhance the elongation but sacrifice the strength to some extent, and the choice of annealing time will depend on the performance of actual need.

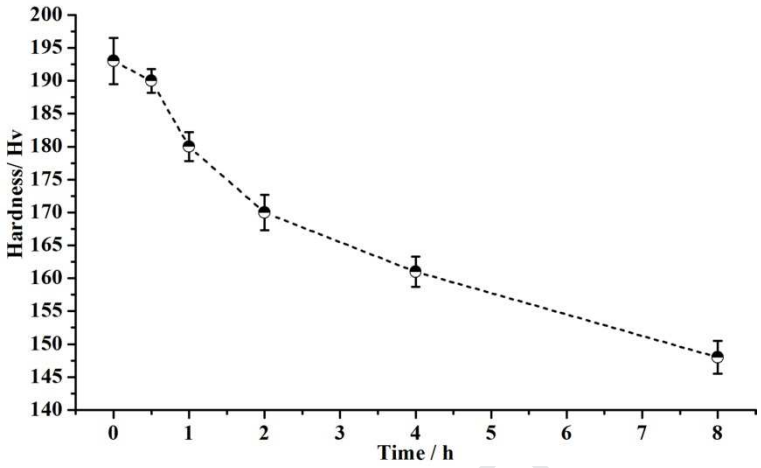

Fig. 11. Variation of the Vickers microhardness of the CR samples as a function of annealing time.

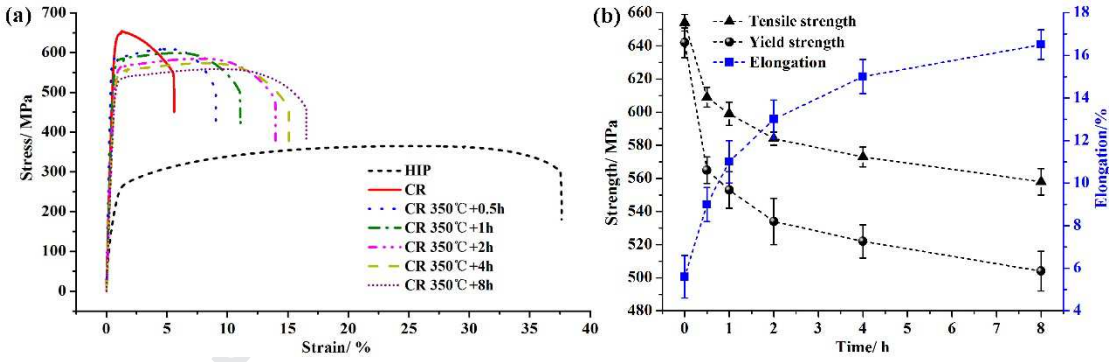

Fig. 12. (a) Typical engineering stress-strain curves of the Cu-3Ag-0.5Zr alloy in different conditions, and (b) effects of annealing time on tensile properties of the CR samples.

The excellent mechanical properties of the Cu-3Ag-0.5Zr alloy mainly result from four mechanisms: precipitation strengthening, dislocation strengthening, grain boundary strengthening, and twin boundary strengthening. First, the high density of nano-sized Ag precipitates can impede the dislocation moving and accumulate dislocations during cold rolling, leading to a high work hardening rate. Meanwhile, it is suggested that the micro-sized Cu_4AgZr particles provide pinning

effects not only to dislocation movement, but also to grain boundary sliding, thus preventing heat treatment induced grain coarsening [15, 18]. Second, the high density of dislocations introduced by cold rolling enhances the strength greatly, but lefts little room for dislocation accumulation during tensile test, resulting in a low elongation of only approximately 5.6%. A significant increment of elongation is observed after annealing since the recovery of dislocation-accumulation ability. Third, according to the classical Hall-Petch relationship, the strength of conventional metals is inversely proportional to the square of grain size [29]. The Cu-3Ag-0.5Zr alloy in this study has a fine microstructure with an average grain size in the range of 0.8-1.8 μm after annealing various times, and the large amounts of ultrafine grains play a vital role in the good combination of high strength and moderate elongation after low-temperature annealing. Lastly, twin boundaries are also considered good sites to accumulate dislocations, which improves the work hardening rate of the alloy and results in an increased elongation after annealing [27, 30].

As a kind of age-hardening alloy, it is to be noted that the Cu-3Ag-0.5Zr alloy subjected to cold rolling displays no enhancement of hardness and strength during annealing at 350 °C, which is not in agreement with the observation of previous literatures [1, 31-33]. The possible reasons are as follows. On the one hand, the high density of dislocations and fine grains after cold rolling provide significant strengthening for the alloy. However, the dislocations are gradually absorbed into the grain boundaries due to the recovery during annealing, leading to the decrease of strength. Meanwhile, a slight coarsening of grains during annealing also results in the softening of the alloy. On the other hand, the initial material has already come close to a peak-aged state before cold rolling, and the precipitates (Ag and Cu_4AgZr) have existed in the CR sample, as evident in Fig. 3 and Fig. 4. Thus, the CR sample loses the potential to enhance the strength through heat treatment.

Conversely, the slight coarsening of the Cu_4AgZr particles after annealing for over 2 h is detrimental to the strength. In addition, the formation of discontinuous Ag precipitates and the dissolution of continuous Ag precipitates in the samples when annealed for over 4 h are also responsible for the drops of hardness and strength.

4 Conclusions

(1) The initial material prepared by gas atomization and HIP shows a fine microstructure with an average grain size of 5.6 μm, which plays a vital role in the formation of ultrafine-grained microstructure in the CR sample.

(2) The high values of hardness (193 Hv), ultimate tensile strength (654 MPa), and yield strength (642 MPa) but a low value of elongation (5.6%) are obtained after cold rolling due to the high density of dislocations and large number of ultrafine grains in the alloy. The interaction between dislocations and fine precipitates (nano-sized Ag and micro-sized Cu_4AgZr) is also responsible for the enhanced strength.

(3) The UTS, YS and EL are 609 MPa, 565 MPa and 9%, respectively, when the CR sample is annealed at 350 ℃ for 0.5 h. After annealing for 2 h, the values of UTS, YS and EL are 584 MPa, 534 MPa and 13%, respectively. Prolonging the annealing time to 8 h, the UTS and YS decrease to 558 MPa and 504 MPa, respectively, while the EL recovers to 16.5%. The decreased strength is associated with the appearance of discontinuous Ag precipitates, the dislocation annihilation and the slight growth of grains during annealing. The increased elongation is mainly attributed to the recovery of dislocation-accumulation ability.

(4) The excellent mechanical properties of the Cu-3Ag-0.5Zr alloy mainly result from the

contribution of four mechanisms: precipitation strengthening, dislocation strengthening, grain boundary strengthening, and twin boundary strengthening.

Acknowledgement

This work was supported by the Science and Technology Plan Projects of Hunan Province, China [2017GK2261].

References

[1] S.C. Krishna, N. Chawake, R.S. Kottada, A.K. Jha, B. Pant, P.V. Venkitakrishnan, High strength and good ductility in Cu-3Ag-0.5Zr alloy by cryo-rolling and aging, J. Mater. Eng. Perform. 26 (2017) 350-357.

[2] Y.Z. Tian, J. Freudenberger, R. Pippan, Z.F. Zhang, Formation of nanostructure and abnormal annealing behavior of a Cu-Ag-Zr alloy processed by high-pressure torsion, Mater. Sci. Eng. A 568 (2013) 184-194.

[3] J.B. Liu, L. Zhang, A.P. Dong, L.T. Wang, Y.W. Zeng, L. Meng, Effects of Cr and Zr additions on the microstructure and properties of Cu-6wt.% Ag alloys, Mater. Sci. Eng. A 532 (2012) 331-338.

[4] J. Lyubimova, J. Freudenberger, C. Mickel, T. Thersleff, A. Kauffmann, L. Schultz, Microstructural inhomogeneities in Cu-Ag-Zr alloys due to heavy plastic deformation, Mater. Sci. Eng. A 527 (2010) 606-613.

[5] S.C. Krishna, K.T. Tharian, B. Pant, R.S. Kottada, Microstructure and mechanical properties of Cu-Ag-Zr alloy, J. Mater. Eng. Perform. 22 (2013) 3884-3889.

[6] X.C. He, Y.M. Wang, H.S. Liu, Z.P. Jin, A study of the isothermal section of the Cu-Ag-Zr ternary system at 1023 K by diffusion triple technique, J. Alloys Compd. 439 (2007) 176-180.

[7] S.C. Krishna, A.K. Jha, B. Pant, K.M. George, Achieving higher strength in Cu-Ag-Zr alloy by warm/hot rolling, Rare Met. 36 (2015) 263-267.

[8] S.C. Krishna, N.K. Gangwar, A.K. Jha, B. Pant, K.M. George, Enhanced strength in Cu-Ag-Zr alloy by combination of cold working and aging, J. Mater. Eng. Perform. 23 (2014) 1458-1464.

[9] X. Wu, R. Wang, C. Peng, Y. Feng, Z. Cai, Effects of annealing on microstructure and mechanical properties of rapidly solidified Cu-3 wt% Ag-1 wt% Zr, Mater. Sci. Eng. A 739 (2019) 357-366.

[10] S. Nestorović, I. Marković, D. Marković, Influence of thermomechanical treatment on the hardening mechanisms and structural changes of a cast Cu-6.6wt.%Ag alloy, Mater. Des. 31 (2010) 1644-1649.

[11] X. Zuo, R. Guo, C. Zhao, L. Zhang, E. Wang, K. Han, Microstructure and properties of Cu-6wt%Ag composite thermomechanical-processed after directionally solidifying with magnetic field, J. Alloys Compd. 676 (2016) 46-53.

[12] D.W. Yao, L.N. Song, A.P. Dong, L.T. Wang, L. Zhang, L. Meng, The role of Ag precipitates in Cu-12wt% Ag, Mater. Sci. Eng. A 558 (2012) 607-610.

[13] X. Wu, R. Wang, C. Peng, Y. Feng, Z. Cai, Influence of hot isostatic pressing and forging on the microstructure and mechanical properties of Cu-3Ag-1Zr alloys, Mater. Des. 168 (2019) 107676.

[14] Y. Wang, M. Chen, F. Zhou, E. Ma, High tensile ductility in a nanostructured metal, Nature 419 (2002) 912-915.

[15] I. Cora, P. Pekker, I. Dódony, D. Janovszky, Single crystal structure determination and refinement of $AgZrCu_4$ and Ag-containing $Cu_{10}Zr_7$ by precession electron diffraction and tomography techniques, J. Alloys Compd. 658 (2016) 678-683.

[16] K. Han, A.A. Vasquez, Y. Xin, P.N. Kalu, Microstructure and tensile properties of nanostructured Cu-25wt%Ag, Acta Mater. 51 (2003) 767-780.

[17] J.B. Liu, L. Meng, Phase orientation, interface structure, and properties of aged Cu-6 wt.% Ag, J. Mater. Sci. 43 (2008) 2006-2011.

[18] G. Chen, C. Wang, Y. Zhang, C. Yi, P. Zhang, Effect of heat treatments on microstructures and tensile properties of Cu-3 wt%Ag-0.5 wt%Zr alloy, Met. Mater. Int. 24 (2018) 255-263.

[19] J. Gubicza, Z. Hegedűs, J.L. Lábár, A. Kauffmann, J. Freudenberger, V. Subramanya Sarma, Solute redistribution during annealing of a cold rolled Cu-Ag alloy, J. Alloys Compd. 623 (2015) 96-103.

[20] K. Sitarama Raju, V. Subramanya Sarma, A. Kauffmann, Z. Hegedűs, J. Gubicza, M. Peterlechner, J. Freudenberger, G. Wilde, High strength and ductile ultrafine-grained Cu-Ag alloy through bimodal grain size, dislocation density and solute distribution, Acta Mater. 61 (2013) 228-238.

[21] M. Bonvalet, X. Sauvage, D. Blavette, Intragranular nucleation of tetrahedral precipitates and discontinuous precipitation in Cu-5wt%Ag, Acta Mater. 164 (2019) 454-463.

[22] N. Kumar, P.N. Rao, R. Jayaganthan, H.-G. Brokmeier, Effect of cryorolling and annealing on recovery, recrystallisation, grain growth and their influence on mechanical and corrosion behaviour of 6082 Al alloy, Mater. Chem. Phys. 165 (2015) 177-187.

[23] W. Wang, F. Brisset, A.L. Helbert, D. Solas, I. Drouelle, M.H. Mathon, T. Baudin, Influence of stored energy on twin formation during primary recrystallization, Mater. Sci. Eng. A 589 (2014)

112-118.

[24] X.P. Chen, L.F. Li, H.F. Sun, L.X. Wang, Q. Liu, Studies on the evolution of annealing twins during recrystallization and grain growth in highly rolled pure nickel, Mater. Sci. Eng. A 622 (2015) 108-113.

[25] D. Field, L. Bradford, M. Nowell, T. Lillo, The role of annealing twins during recrystallization of Cu, Acta Mater. 55 (2007) 4233-4241.

[26] G.K. Williamson, W.H. Hall, X-ray line broadening from filed aluminium and wolfram, Acta Mater. 1 (1953) 22-31.

[27] J. Li, B. Gao, Y. Wang, X. Chen, Y. Xin, S. Tang, B. Liu, Y. Liu, M. Song, Microstructures and mechanical properties of nano carbides reinforced CoCrFeMnNi high entropy alloys, J. Alloys Compd. 792 (2019) 170-179.

[28] Y.H. Zhao, X.Z. Liao, Z. Jin, R.Z. Valiev, Y.T. Zhu, Microstructures and mechanical properties of ultrafine grained 7075 Al alloy processed by ECAP and their evolutions during annealing, Acta Mater. 52 (2004) 4589-4599.

[29] E.O. Hall, The deformation and ageing of mild steel: III discussion of results, Proc. Phys. Soc. London B 64 (1951) 747-753.

[30] P. Sathiyamoorthi, J. Moon, J.W. Bae, P. Asghari-Rad, H.S. Kim, Superior cryogenic tensile properties of ultrafine-grained CoCrNi medium-entropy alloy produced by high-pressure torsion and annealing, Scr. Mater. 163 (2019) 152-156.

[31] H. Fu, S. Xu, W. Li, J. Xie, H. Zhao, Z. Pan, Effect of rolling and aging processes on microstructure and properties of Cu-Cr-Zr alloy, Mater. Sci. Eng. A 700 (2017) 107-115.

[32] S. Zhang, R. Li, H. Kang, Z. Chen, W. Wang, C. Zou, T. Li, T. Wang, A high strength and high electrical conductivity Cu-Cr-Zr alloy fabricated by cryorolling and intermediate aging treatment, Mater. Sci. Eng. A 680 (2017) 108-114.

[33] I. Marković, S. Ivanov, U. Stamenković, R. Todorović, A. Kostov, Annealing behavior of Cu-7at.%Pd alloy deformed by cold rolling, J. Alloys Compd. 768 (2018) 944-952.

No conflict of interest exits in this paper, and the paper is approved by all authors for publication. I would like to declare that the work described in this paper is our original research that has not been published in any form previously, and not under consideration for publication elsewhere, in whole or in part. All the authors listed have approved the paper that is enclosed.